Emergent Chiral Spin Liquid: Fractional Quantum Hall Effect in a Kagome Heisenberg Model: Supplementary Information

Shou-Shu Gong, Wei Zhu, and D. N. Sheng
Department of Physics and Astronomy, California State University, Northridge, California 91330, USA.

I. TOPOLOGICAL DEGENERATE GROUND-STATE ENERGY

In the gapped topological states, the ground-state energies in different topological sectors are near degenerate on finite-size systems. With the increase of the system width, the difference of the near degenerate energies vanishes exponentially. In the density-matrix renormalization group (DMRG) calculations, we obtain the bulk energy per site in both the vacuum (E_1^0/N) and spinon (E_1^S/N)sectors by subtracting the energies of two long cylinders with different system lengths in each sector. $(E_1^S - E_1^0)/N$ describes the difference of the ground-state energies in different topological sectors.

Here, we show the results for $J' = 0.5$ on $L_y = 4$ cylinder in Suppl. Table. I. By keeping the unconverged 2000 $SU(2)$ states, we find a small energy difference 0.00008. And with increasing kept states, the difference continues to decrease. For the well converged ground states with the DMRG truncation error $\epsilon \simeq 1 \times 10^{-7}$ by keeping 5000 $SU(2)$ states, we show the energy difference is 0.00001, which is consistent with the exact diagonalization results shown below and the topological degeneracy in the system. This energy splitting 0.00001 is much smaller than that in the nearest-neighbor (NN) kagome Heisenberg model 0.00069.

II. TOPOLOGICAL ENTANGLEMENT ENTROPY

For the gapped quantum states with topological order, the topological entanglement entropy (TEE) γ is proposed to characterize the non-local entanglement. The Renyi entropy of a subsystem A with reduced density matrix ρ_A are defined as $S_n = (1-n)^{-1}\ln(\mathrm{Tr}\rho_A^n)$, where the $n \to 1$ limit gives the Von Neuman entropy. For a topologically ordered state, Renyi entropy has the form $S_n = \alpha L - \gamma$, where L is the boundary of the subsystem, and all other terms vanish in the large L limit; α is a non-universal constant, while a positive γ is a correction to the area law of entanglement and reaches a universal value determined by total quantum dimension D of quasiparticle excitations as $\gamma = \ln D$. For the $\nu = 1/2$ Laughlin state, the quantum dimension of each quasiparticle is 1, leading to the total dimension $D = \sqrt{2}$ and thus the TEE $\gamma = \ln 2/2$.

By using the complex number DMRG simulations, we obtain the minimal entropy state (MES) with spontaneously broken time-reversal symmetry and the corresponding Von Neuman entanglement entropy. With the help of the $SU(2)$ DMRG, we could obtain the converged entropy for $L_y = 3, 4, 5$ cylinders. For $L_y = 6$ cylinder, we cannot get the converged entropy because the required DMRG optimal state number $M_{\mathrm{SU}(2)}$ is beyond our computation abilities. Thus, to find an estimation of the entropy on $L_y = 6$ cylinder, we study the entropy versus $1/M_{\mathrm{SU}(2)}$ as shown in Fig. 1(a), and make a careful extrapolation of the data to estimate the converged result. For $J' = 0.5$, we find the entropy $S = 4.49 \pm 0.02$. In Fig. 1(b), we make a linear fitting of the entropy data for $L_y = 4, 5, 6$ cylinders at $J' = 0.5$, and find the TEE $\gamma = 0.34 \pm 0.04$, which is consistent with the TEE of the $\nu = 1/2$ Laughlin state $\gamma = \ln 2/2$.

III. SPIN-SPIN CORRELATION FUNCTION

For a gapped topological chiral spin liquid (CSL), the system is expected to have a short-range spin correlation. We measure the spin-spin correlation function on the cylinders with $L_y = 4$ and 6 for both vacuum and spinon sectors. We demonstrate

$J' = 0.5, L_y = 4$	E_1^0/N	E_1^S/N	$(E_1^S - E_1^0)/N$
$M_{\mathrm{SU}(2)} = 2000$	-0.46046	-0.46038	0.00008
$M_{\mathrm{SU}(2)} = 4000$	-0.46050	-0.46048	0.00002
$M_{\mathrm{SU}(2)} = 5000$	-0.46052	-0.46051	0.00001

TABLE I: **Degenerate ground-state energies in the different topological sectors**. The ground-state energy per site in both the vacuum (E_1^0/N) and spinon (E_1^S/N) sectors, as well as the energy difference between the two sectors $(E_1^S - E_1^0)/N$ for $J' = 0.5$ on the $L_y = 4$ cylinder. To avoid edge effects, these bulk energies are obtained by subtracting the energies of two long cylinders with different system lengths. $M_{\mathrm{SU}(2)}$ is the kept $SU(2)$ states.

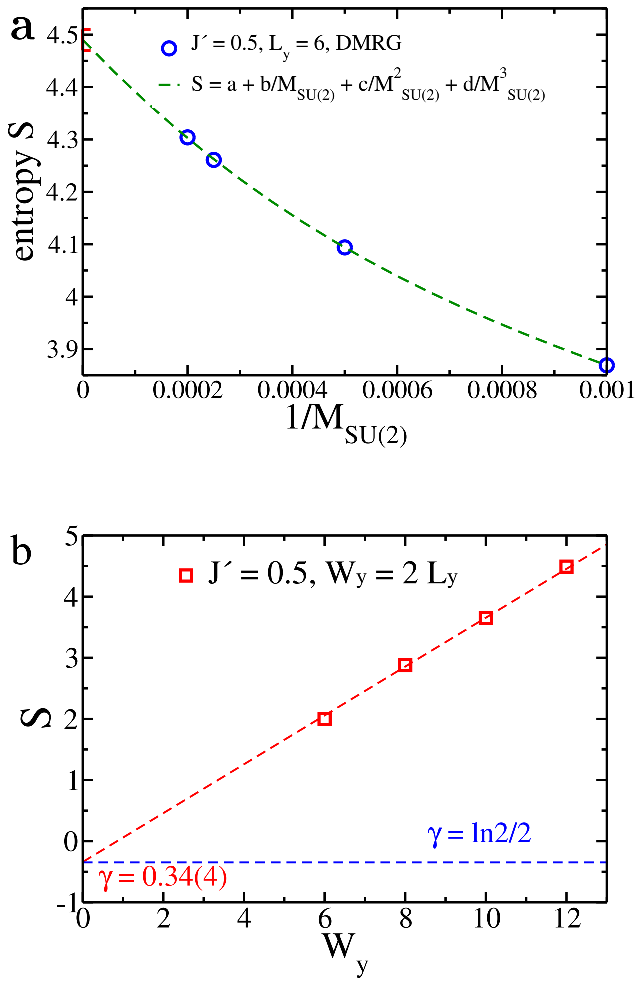

FIG. 1: **Topological entanglement entropy**. (a) Entanglement entropy S versus DMRG optimal state number inverse $1/M_{\mathrm{SU}(2)}$ for $J' = 0.5$ on $L_y = 6$ cylinder. The DMRG entropy is for the MES, which is obtained from the complex number DMRG simulations. The data are fitted using the formula $S = a + b/M_{\mathrm{SU}(2)} + c/M^2_{\mathrm{SU}(2)} + d/M^3_{\mathrm{SU}(2)}$, from which we find the convergent entropy $S = 4.49 \pm 0.02$. (b) Entanglement entropy versus system width for $J' = 0.5$. By a linear fitting of the results for $L_y = 4, 5, 6$, we find the TEE $\gamma = 0.34 \pm 0.04$, where the error bar is from the uncertainty of the entropy on $L_y = 6$ cylinder as shown in (a). The TEE we find is consistent with the result of the $\nu = 1/2$ Laughlin state $\gamma = \ln 2/2$.

$\langle S_i \cdot S_j \rangle$ with site i in the center of lattice and j along the same row from the bulk to the boundary for $J' = 0.5$ in Suppl. Fig. 2. The spin correlations exhibit the exponential decay in both vacuum and spinon sectors. And the decay length does not increase with growing L_y from 4 to 6, which suggests that the spin correlation length is close to saturation with growing system width. This observation is consistent with a vanishing magnetic order.

IV. VALENCE-BOND SOLID ORDER

To investigate the possible valence-bond solid (VBS) order, we study the dimer-dimer correlation function on cylinder systems, which is defined as

$$D_{(i,j),(k,l)} = 4[\langle (\vec{S}_i \cdot \vec{S}_j)(\vec{S}_k \cdot \vec{S}_l) \rangle - \langle \vec{S}_i \cdot \vec{S}_j \rangle \langle \vec{S}_k \cdot \vec{S}_l \rangle], \tag{1}$$

where (i, j) and (k, l) represent the nearest-neighbor (NN) bonds. First of all, we demonstrate the real space distributions of the NN bond energies on cylinder systems. To clearly show the fluctuations of the NN bond energies, we define the bond texture as the bond energies subtracting a constant e, which is the average NN bond energy in the bulk of cylinder, i.e., $B_{i,j} = \langle S_i \cdot S_j \rangle - e$.

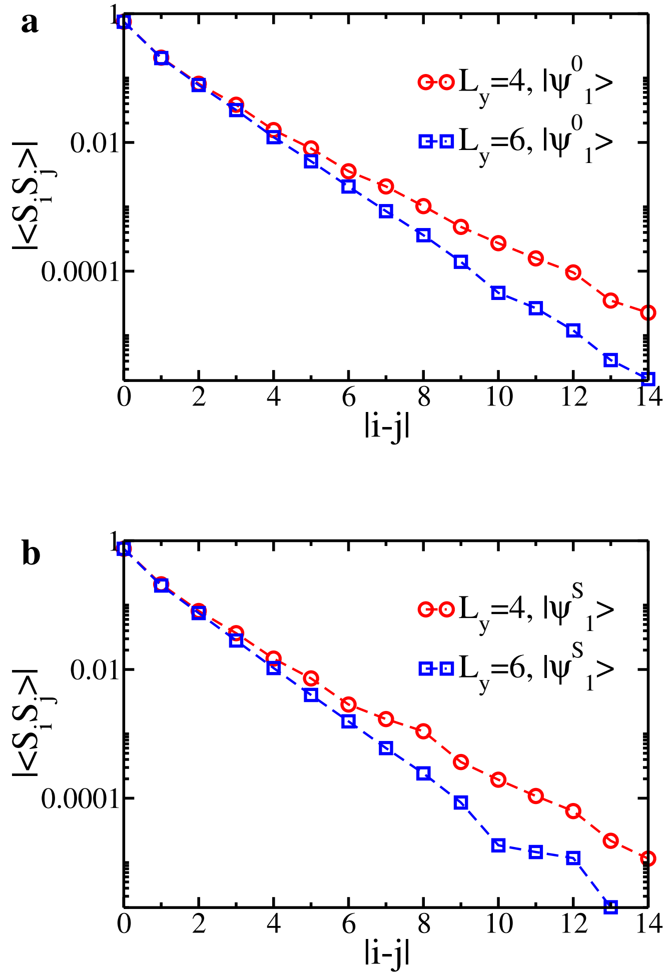

FIG. 2: **Spin-Spin correlation function**. Log-linear plot of the absolute value of the spin-spin correlation function versus the distance of sites $|i-j|$ on $3 \times 24 \times 4$ and $3 \times 24 \times 6$ cylinders for $J' = 0.5$ in (a) vacuum and (b) S-sectors. The reference site i is located in the center of cylinder, and site j is chosen along the same row from the bulk to the boundary.

As shown in Suppl. Fig. 3 of the bond textures on $3 \times 16 \times 4$ cylinders for $J' = 0.5$ in the vacuum sector, we obtain the uniform bond textures along both the x and y directions in the bulk of cylinders. The small differences between the x and y bond textures 0.01 and 0.004 in Suppl. Figs. 3(a) and 3(b) are owing to the long cylinder geometry, which breaks the lattice rotation symmetry. The uniform bond textures indicate the good convergence of our DMRG results.

With the uniform bond textures in the bulk, we could further study the dimer-dimer correlation functions. We set the reference bond (i, j) in the middle of cylinder. Suppl. Fig. 4 shows the dimer-dimer correlations on the $3 \times 16 \times 4$ cylinders at $J' = 0.5$ in the vacuum sector. The black bond in the middle denotes the reference bond (i, j), and the red and blue bonds indicate the negative and positive dimer correlations, respectively. We show that the dimer-dimer correlations decay quite fast to zero in both x and y directions. On the $3 \times 18 \times 6$ cylinders, the dimer correlations have a similar fast decay. The significant short-range dimer correlations strongly indicate the vanishing VBS order.

For $J' \geq 0.8$, we find a strong VBS state with breaking lattice translational symmetry in the system. As demonstrated in Suppl. Fig. 5 of the bond textures at $J' = 1.0$ on a $3 \times 16 \times 4$ cylinder, the horizontal NN bond textures are not uniform in the bulk of cylinder but have a difference of 0.01, and the tilt bonds along the vertical direction also have a difference of 0.01, which are quite different from the uniform state in the CSL phase as shown in Suppl. Fig. 3(b). These observations indicate that we find the ground state with lattice translational symmetry breaking in both the x and y directions.

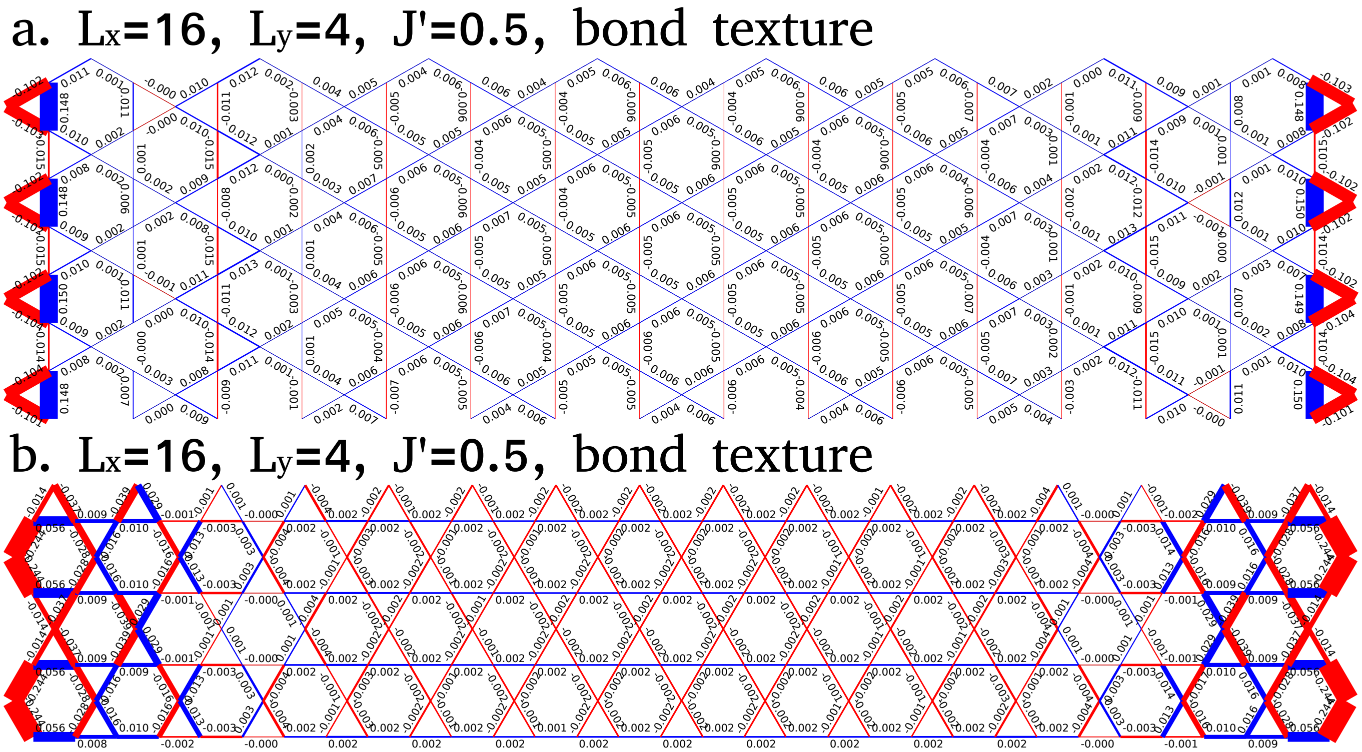

FIG. 3: **Nearest-neighbor bond textures at** $J' = 0.5$. The NN bond textures $B_{i,j}$ on the $3 \times 16 \times 4$ cylinders at $J' = 0.5$ in the vacuum sector. The numbers denote the amplitudes of bond texture $B_{i,j} = \langle S_i \cdot S_j \rangle - e$, where e is the average NN bond energy in the bulk of cylinder. Here, we find $e = -0.212$ and -0.210 for (a) and (b), respectively. The blue (red) color represents the positive (negative) bond texture.

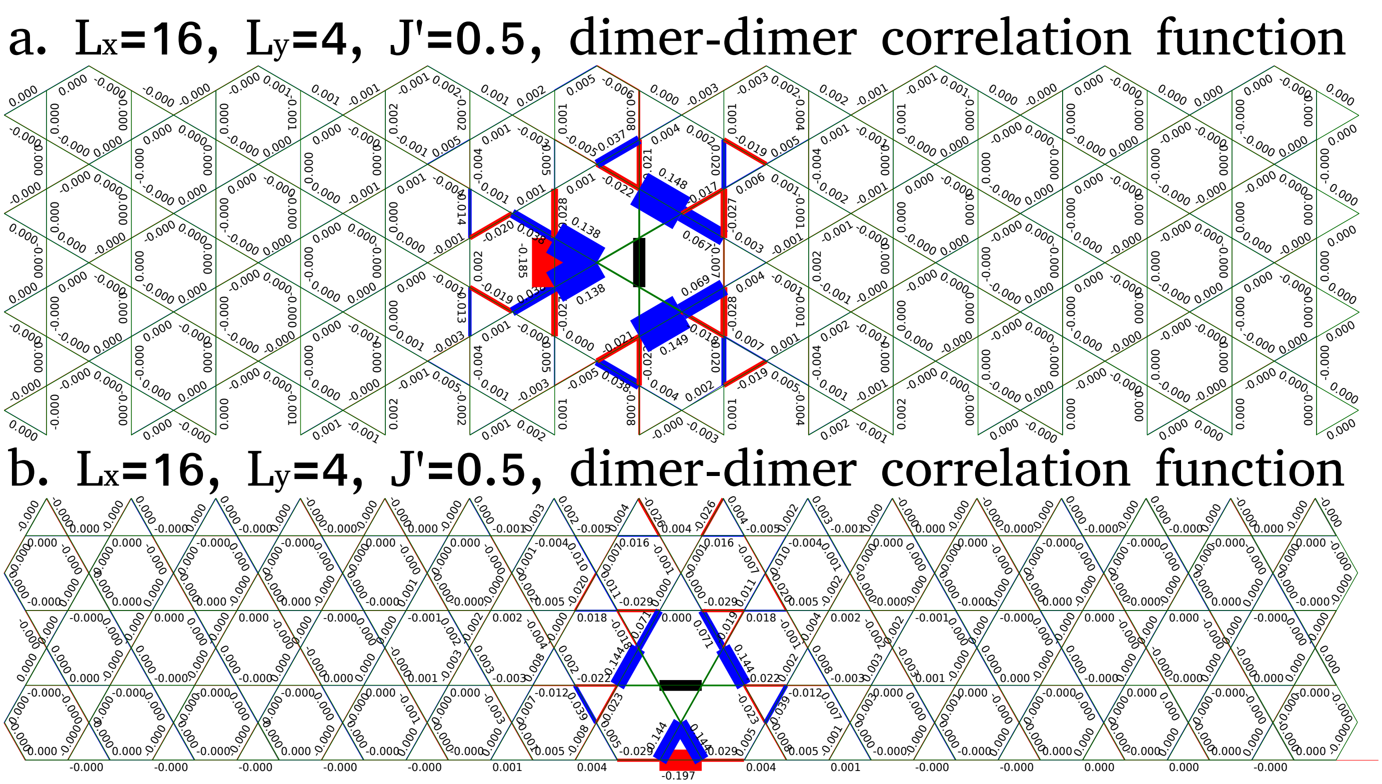

FIG. 4: **Dimer-Dimer correlation function at** $J' = 0.5$. Dimer-Dimer correlation for $J' = 0.5$ on the $3 \times 16 \times 4$ cylinders in the vacuum sector. The black bond in the middle of cylinder denotes the reference bond (i, j). The blue and red bonds represent the positive and negative dimer correlations, respectively.

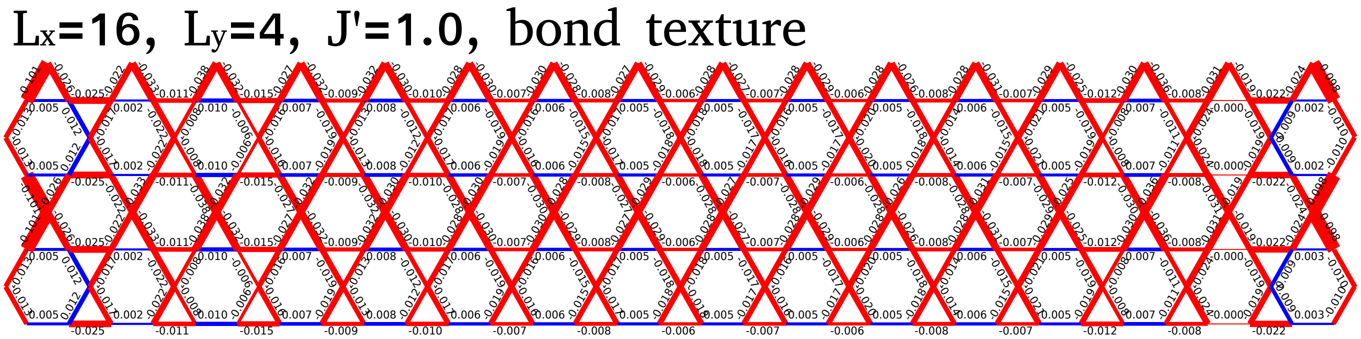

FIG. 5: **Nearest-neighbor bond textures at** $J' = 1.0$. The NN bond textures $B_{i,j}$ on the $3 \times 16 \times 4$ cylinder at $J' = 1.0$. The numbers denote the amplitudes of bond texture $B_{i,j} = \langle S_i \cdot S_j \rangle - e$, where e is the average of the horizontal NN bond energy in the bulk of cylinder. Here, we find $e = -0.0385$. The blue (red) color represents the positive (negative) bond texture.

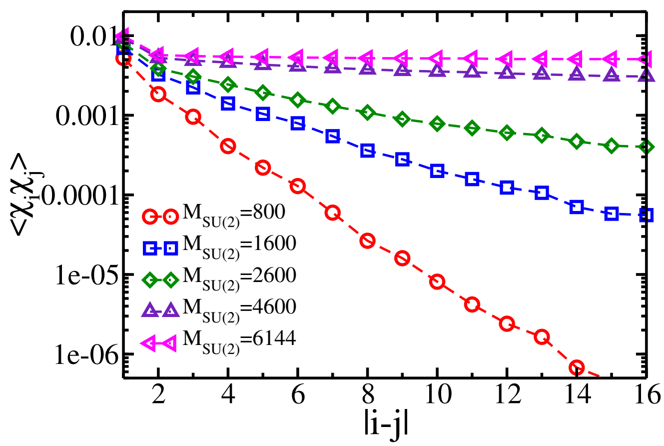

FIG. 6: **Chiral-Chiral correlation function**. The improvement of chiral-chiral correlation function with the growing DMRG optimal states for a $3 \times 18 \times 6$ cylinder at $J' = 0.2$ in the vacuum sector. $M_{\mathrm{SU}(2)}$ is the kept $SU(2)$ states for obtaining the different chiral correlations, which are equivalent to about 3200, 6400, 10000, 18000, and 24000 $U(1)$ states.

V. CHIRAL-CHIRAL CORRELATION FUNCTION

In the DMRG calculations of chiral-chiral correlation function, the systems near phase boundaries require much more kept states than in deep of the CSL region to capture the long-range chiral correlations. As shown in Suppl. Fig. 6 of the improvement of chiral correlation function with the growing DMRG kept states for a $N = 3 \times 18 \times 6$ cylinder at $J' = 0.2$ in the vacuum sector, the system shows a fast exponential decay chiral correlation by keeping 800 $SU(2)$ states (equivalent to about 3200 $U(1)$ states), and with increasing kept states the decay length continues to grow. When keeping 4600 $SU(2)$ states (equivalent to about 18000 $U(1)$ states), the chiral correlations form a long-range correlation. Meanwhile, we only need to keep about 10000 $U(1)$ states to uncover the long-range chiral correlations in deep of the CSL region such as at $J' = 0.4, 0.5$. Therefore, the less convergent DMRG calculations may find a narrower CSL phase region.

VI. EXACT DIAGONALIZATION RESULTS

A. Lowest-Energy spectrum for 36-sites torus

We calculate the low-energy spectrum of the $J - J'$ model on a 36 sites kagome lattice using exact-diagonalization (ED) method. We consider a finite system with periodic boundary conditions, as shown in Suppl. Fig. 7(a). For this geometry, the two-fold topological degeneracy of the $\nu = 1/2$ FQHE are expected to live in the momentum sectors $\mathbf{k} = (0, 0)$ and $(0, \pi)$.

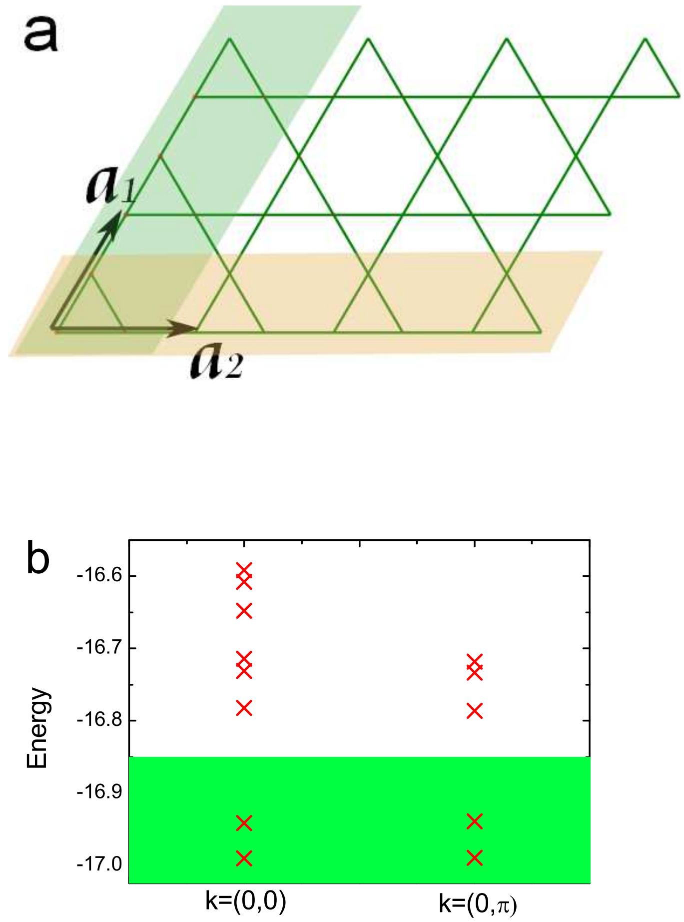

FIG. 7: (a) Geometry of the 36 sites kagome lattice with lattice constant $\vec{a}_1, \vec{a}_2$. (b) Low-energy spectrum in the momentum space $\mathbf{k} = (0,0), (0,\pi)$ at $J' = 0.6$.

Thus we obtain the low-energy spectrum in these two momentum subspaces. As shown in Suppl. Fig. 7(b) of the spectrum at $J' = 0.6$, we find that two lowest states for each momentum sector, denoted by $E_1^{k=0(\pi)}, E_2^{k=0(\pi)}$, are well separated from the continuum of other excitations by a gap that is about 0.15. The nearly vanishing energy difference between two sectors $E^0_{1(2)} - E^{\pi}_{1(2)} = 0.0007(0.0022)$ indicates the emergence of the many-body magnetic translational symmetry. The existence of the two lowest states in each sector is due to the time reversal symmetry. Therefore, our ED calculations imply that the system has four-fold degeneracy of ground states, where two of them are from topological degeneracy and two are from time reversal symmetry.

B. Modular matrix

The information of quantum dimension and fusion rules of the quasiparticles are encoded in the modular $\mathcal{S}$ matrix. To extract the modular $\mathcal{S}$ matrix in our model, we use the method of searching the minimal entropy states (MESs) to construct the modular matrix. In this method, we first calculate the entanglement entropy through partitioning the full torus system into two subsystems (cylinders) A and B then tracing out the subsystem B. Here we consider two noncontractible bipartitions on torus geometry as shaded by light green and brown in Suppl. Fig. 7(a), which is along the lattice vectors $\vec{a}_1, \vec{a}_2$, respectively.

We denote the four groundstates from ED calculation as,

$$|\psi_1^{k=0}\rangle, |\psi_2^{k=0}\rangle, |\psi_1^{k=\pi}\rangle, |\psi_2^{k=\pi}\rangle. \tag{2}$$

Here, each wavefunction is being chosen as a real one. All the above four groundstates preserve the time reversal symmetry and

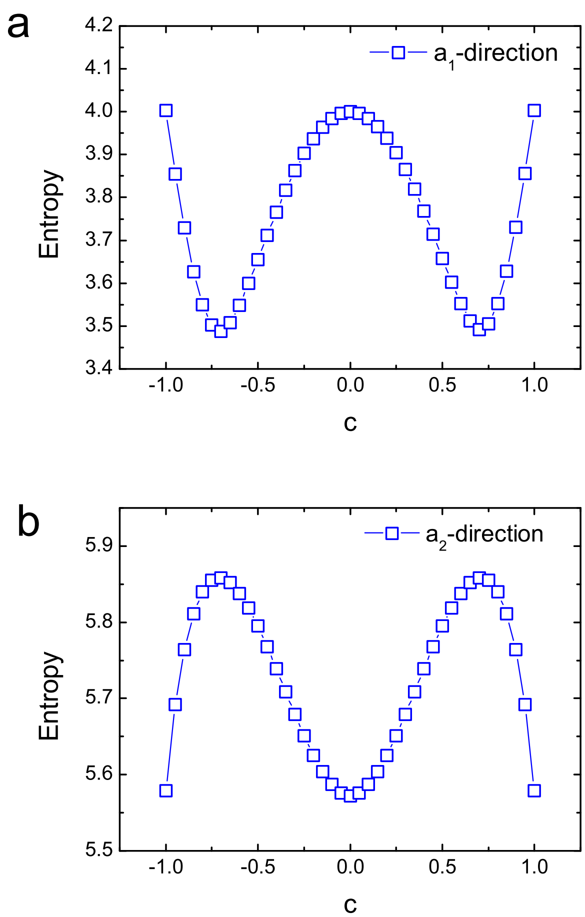

FIG. 8: Entropy for the superposition state $|\Psi\rangle = c|\tilde{\psi}_L^{k=0}\rangle + \sqrt{1-c^2}|\tilde{\psi}_L^{k=\pi}\rangle$ for the partition along (a) a_1-direction and (b) a_2-direction. The black arrows show parameters for the MESs.

show a vanishing chiral order. According to the discussions in main text, we can construct the chiral states in each sector as

$$|\tilde{\psi}_{L,R}^{k=0}\rangle = \frac{1}{\sqrt{2}}(|\psi_1^{k=0}\rangle \pm i|\psi_2^{k=0}\rangle) \tag{3}$$

$$|\tilde{\psi}_{L,R}^{k=\pi}\rangle = \frac{1}{\sqrt{2}}(|\psi_1^{k=\pi}\rangle \pm i|\psi_2^{k=\pi}\rangle) \tag{4}$$

where $L(R)$ represents the left (right) chirality.

Then we use two chiral states with the same chirality, for example $|\tilde{\psi}_L^{k=0}\rangle$ and $|\tilde{\psi}_L^{k=\pi}\rangle$, to calculate the modular matrix. We search for the MESs in the space of the groundstate manifold using the following superposition wavefunction:

$$|\Psi\rangle = c|\tilde{\psi}_L^{k=0}\rangle + \sqrt{1-c^2}e^{i\phi}|\tilde{\psi}_L^{k=\pi}\rangle,$$

where $c \in [0,1]$ and $\phi \in [0,2\pi]$ are the superposition parameters. In our calculation, we find that the global MESs take $\phi = 0$. As shown in Suppl. Fig. 8, the two orthogonal MESs along a_1-direction are respectively located at $c = \frac{1}{\sqrt{2}}$ and $c = -\frac{1}{\sqrt{2}}$, while the MESs along a_2-direction occur at $c = 0, 1$. Therefore, we have two MESs along a_1-direction

$$|\Xi_1^{a_1}\rangle = \frac{1}{\sqrt{2}}(|\tilde{\psi}_L^{k=0}\rangle + |\tilde{\psi}_L^{k=\pi}\rangle), \tag{5}$$

$$|\Xi_2^{a_1}\rangle = \frac{1}{\sqrt{2}}(|\tilde{\psi}_L^{k=0}\rangle - |\tilde{\psi}_L^{k=\pi}\rangle), \tag{6}$$

and the two MESs along a_2-direction,

$$|\Xi_1^{a_2}\rangle = |\tilde{\psi}_L^{k=0}\rangle, \tag{7}$$
$$|\Xi_2^{a_2}\rangle = |\tilde{\psi}_L^{k=\pi}\rangle. \tag{8}$$

The modular $\mathcal{S}$ matrix is obtained from the overlaps between the MESs of the two noncontractible partition directions:

$$\mathcal{S} = \langle \Xi^{a_1} | \Xi^{a_2} \rangle = \frac{1}{\sqrt{2}} \begin{pmatrix} 1 & 1 \\ 1 & -1 \end{pmatrix}, \tag{9}$$

which is consistent with the prediction of $SU(2)_1$ conformal field theory about the $\nu = 1/2$ bosonic Laughlin state. Through the modular matrix above, we can extract the individual quantum dimension $d_{\mathbb{1}(s)} = 1$ for quasiparticle $\mathbb{1}(s)$ and the fusion rules $\mathbb{1} \times \mathbb{1} = \mathbb{1}$, $\mathbb{1} \times s = s$, $s \times s = \mathbb{1}$, which also determine the characteristic semion statistics of the s quasiparticle.